PAPER

A facile one-step process for 3D N-doped noncovalent functionalization PS/rGO composites

Materials Research Express

PAPER

A facile one-step process for 3D N-doped noncovalent functionalization PS/rGO composites

RECEIVED
20 January 2017

REVISED
17 February 2017

ACCEPTED FOR PUBLICATION
3 March 2017

PUBLISHED
22 March 2017

Weiqi Huang[1,2], Hua Wang[1], Zheng Su[1,2], Konghu Tian[1,2], Xianzhu Ye[1], Chao Bao[1], Yulan Guo[1,2], Jing He[1,2] and Xingyou Tian[1]

[1] Institute of Applied Technology, Hefei Institutes of Physical Science, Chinese Academy of Sciences, Hefei 230031, People's Republic of China
[2] University of Science and Technology of China, Hefei 230026, People's Republic of China

E-mail: wanghua@issp.ac.cn

Keywords: graphene, 3D, N, N-dimethylformamide solvothermal, nitrogen doping

Abstract

This work reports a simple, versatile and facile one-step process to prepare the three-dimensional (3D) N-doped noncovalent functionalization polystyrene/reduced graphene oxide (PS/rGO) composites. In this, N, N-dimethylformamide (DMF) acts as the solvent, reducing agent, and more importantly, the N-doping agent. Various measurements have been carried out to characterize the structure and morphology of PS/rGO composites, in particular for the excellent electrical conductivity of PS/rGO composites compared with virgin PS, which was attributed to the 3D pores structure and the N-doping. With regards to the unique properties of graphene, the 3D framework structure and the N-doping, this composite material has great potential properties such as electromagnetic interference shielding effectiveness (EMI) to be explored.

1. Introduction

Graphene is a single atom-thick layer sp^2-bonded carbon atoms of two-dimensional (2D) honeycomb lattice carbon material, and has attracted extensive interest since 2004 due to outstanding properties such as large specific surface area, charge carrier mobility, preeminent mechanical strength, excellent electrical and thermal conductivities, and excellent stability [1–3]. A large number of works have indicated the tremendous potential of graphene in many scientific fields, for instance chemical and biological sensors, electrocatalysis, polymer composites, energy-storage materials and environmental protection materials, etc [4, 5].

In recent years, a lot of work has been devoted to the 2D graphene nanosheets/polymer composites into three-dimensional (3D) network-based materials, such as hydrogels, aerogels, sponges and some other pores structures [6, 7]. The 2D structure of polymer/graphene composites in general sacrifices the unique properties of graphene nanosheets, and the graphene sheets were more easy to restack and aggregate on account of the π–π interaction, van der Waals force and hydrophobic interaction. But the 3D framework structures could solve these above-mentioned problems and retain the unique properties of individual graphene sheets, such as high specific surface areas etc, to a certain extent [8, 9]. So far, there are some strategies that have been reported for fabricating 3D graphene-based architecture materials including template-directed methods, like the template-directed CVD method and template-directed assembly method [10, 11], electrochemical synthesis [12], etc. These strategies are all complex and need special facilities. In addition, most of the 3D polymer/graphene composites were dried by supercritical fluid drying and freeze-drying, which were expensive and relatively time-consuming [13, 14].

In this work, a simple, versatile and facile one-step process for the preparation of the noncovalent functionalization polystyrene/reduced graphene oxide (PS/rGO) composite with 3D framework networks is reported. In the N, N-dimethylformamide (DMF) solvothermal process, the graphene oxide (GO) could be reduced in-situ without extra deoxidizers like NH_4OH [15], hydrazine monohydrate etc [16], thus achieving the noncovalent functionalization PS/rGO composite through the strong π–π interaction. Furthermore, the DMF not only was used to dissolve the PS, but could provide the nitrogen (N) source to achieve N-doping without extra N-doping agents like melamine [17], ammonia etc [18]. And the samples of this work were dried by a flexible ambient-pressure-drying that was cheaper and safer, which could also achieve the same effect as the supercritical fluid dry-

ing or freeze-drying. In summary, the 3D noncovalent functionalization PS/rGO composites were prepared by a simple DMF solvothermal reaction and ambient-pressure-dried, without extra deoxidizers and N-doping agents. With regards to the unique properties of graphene, the PS/rGO composites potential properties will be explored.

2. Experimental

2.1. Preparation of GO

The GO was synthesized from natural graphite powder (average area: 2025 μm^2, Qingdao Huatai Lubricant Sealing S&T Co. Ltd) according to the modified Hummers' method [19, 20]. For the method, concentrated sulfuric acid (75 ml), the graphite powder (1 wt equiv) and $NaNO_3$ (0.75 wt equiv) were added to a 250 ml bottle equipped with a treater, and put into an ice bath to control the temperature to below 5 °C. Then the $KMnO_4$ (3 wt equiv) was added slowly to keep the reaction temperature below 10 °C. After that, the reaction temperature was increased to 35 °C in 2 h, then the suspension was stirred for 2 d. Deionized water (140 ml) was added slowly to deliquate the suspension, then the reaction temperature was increased to 80 °C for 30 min. 30% H_2O_2 (10 ml) was added into the bottle after the temperature was cooled to room temperature. The mixture was centrifuged and washed with 5% HCl solution, deionized water for three times to purify the GO. The concentration of GO was about 5.0 mg · ml^{-1}, which was confirmed four times by the drying GO solution at 60 °C for 12 h.

2.2. Preparation of 3D self-assembly PS/rGO

The PS/rGO composites were prepared according to a facile one-pot self-assembly N, N-dimethylformamide (DMF) solvothermal method. The PS (molecular weight $M_w = 142$ kg mol^{-1} and $M_n/M_w = 1.21$ was offered by Yangzi-BASF Styrenics Co., Ltd) was dissolved in the DMF. And the GO (40, 50, 60, 70, 80, 90, 100 mg) aqueous solution was displaced to GO DMF solution by stirring in the water bath at 80 °C for several hours which must ensure total replacement. Then the PS solution was mixed with the GO solution to 50 ml DMF solution, followed by ultrasonication for 1 h. If there was water remaining in the GO DMF solution, the PS precipitated from the mixture. The mixture containing PS and different concentrations of GO was sealed in a 100 ml Teflon-lined autoclave and retained at 180 °C for 12 h. The amounts of GO were 4 wt.%, 5 wt.%, 6 wt.%, 7 wt.%, 8 wt.%, 9 wt.% and 10 wt.% of the PS, which were labeled as 4, 5, 6, 7, 8, 9, and 10 respectively. The as-prepared cylindrical hydrogels were taken out when the autoclave was cooled to room temperature. Then the samples were washed, soaked in ethanol at room temperature and 50 °C for several days. The as-prepared black hydrogel was solvent-exchanged with ethanol to remove the DMF dissolvant as much as possible [21]. Finally, the composites were dried at room temperature and ambient pressure. For comparison, the rGO was prepared the same way.

2.3. Characterization

The morphologies of the samples were observed via a Sirion-200 (FEI, America) scanning electron microscopy (SEM) with an accelerating voltage of 20 kV. The morphology of PS/rGO were characterized via transmission emission microscopy (JEM-2010 TEM) which was equipped with energy dispersive spectroscopy (EDS). X-ray film and powder diffraction (XRD) patterns were carried out by a Philips X'Pert Pro MPD x-ray diffractometer (40 kV, 40 mA) with Cu Ka radiation ($k = 0.154$ nm), with 2θ mode range of 5–80° at a scan speed of 10° min^{-1}. XPS of the GO and composite 10 were obtained via an x-ray photoelectron spectroscopy (American Thermo ESCALAB 250). Infrared (IR) spectra were measured by a Nicolet 8700 FTIR spectrometer (Thermo Scientific Instrument Co. USA). A Confocal Raman Microscopy (Renishaw inVia Reflex) with an excitation wavelength of 532 nm was used to measure the Raman spectra of specimens. The electrical conductivity of cylindrical samples were measured by a digital, four-point probe RTS-9 resistivity measurement system at room temperature. Thermal properties of samples were characterized by thermal gravimetric analysis (TGA) using a Q5000 IR thermal gravimetric analyzer at a heating rate of 10 °C min^{-1} under nitrogen and nitrogen conditions from 50–700 °C. High volume resistivity beyond $10^6\ \Omega \cdot cm$ for example pure PS ($20 \times 15 \times 5\ mm^3$) was measured by high resistivity meter LK2679A. The data of specimens were from the average of three measurements. The frequency dependence of EMI shielding effectiveness of the samples which were the toroidal shaped samples with an outer diameter of 7.00 mm and inner diameter of 3.00 mm were measured via a AV3629A vector network analyzer with 300 kHz to 9 GHz.

3. Results and discussion

3.1. Preparation process

The overall procedure for preparing for PS/rGO composites is illustrated in scheme 1. The GO was synthesized by the the modified Hummers' method. The PS/rGO composites were synthesized by a simple DMF solvothermal process in a 100 ml sealed Teflon-lined stainless-steel autoclave at 180 °C after 12 h. DMF was decomposed into carbon monoxide (CO) and dimethylamine ($NH(CH_3)_2$) at the DMF solvothermal process (chemical reaction formula in scheme 1). It is proverbial that carbon monoxide is a good reducing agent, which can efficaciously

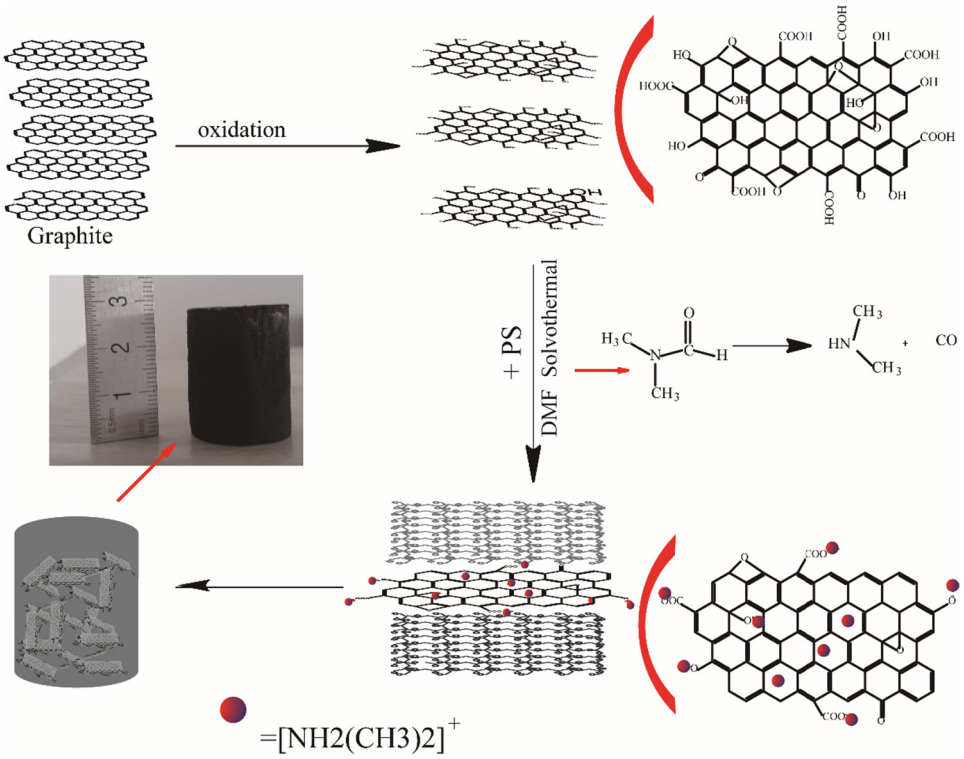

Scheme 1. Illustration of the formation process of GO and the solvothermal self-assembly of PS/rGO composites. Inset: digital image of the sample (4).

remove oxygen from GO. So, the GO could be reduced into rGO via carbon monoxide chemical reduction and thermal reduction, which has been known as the reduction of GO at the DMF solvothermal reaction. On the other hand, dimethylamine ($NH(CH_3)_2$) could be intuitively determined by how the color of solution turned to yellow and the smell of amine after the reaction. As a result of protonation, $NH(CH_3)_2$ could become positively charged in the shape of $[NH_2(CH_3)_2]^+$. And the $[NH_2(CH_3)_2]^+$ could interact with the negatively charged like COO^-, O^- etc, which are residual in the rGO sheet driven by electrostatic interaction [22, 23]. The PS chain was binded and adhesed on the surfaces of rGO through the strong π–π interaction. The formation of noncovalent cross-linking sites of the framework of the 3D PS/rGO resulted from the partial overlapping or coalescing of flexible rGO sheets, then the 3D networks was formed by multifarious interactions including the strong π–π stacking interaction, the physical twine of the rGO sheets, and hydrogen bonding [24, 25].

3.2. Structure and morphology

Figures 1(a)–(d) show the investigation of the morphology and microstructure of sample 4, 6, 8, and 10 via SEM. For these composites, a well-defined and 3D pore architecture which has randomly opened micropores could be distinctly observed from figures 1(a)–(d). The sizes of the pores are from submicrometer to several micrometers and the walls of the randomly opened micropores consisted of thin layers of stacked reduced graphene sheets. Similar morphology and microstructure were reported in other literature [26, 27]. The TEM and EDS analysis were used to further explore the morphology and microstructure of the samples. The selected-area electron diffraction pattern (SAED) of graphene oxide was exhibited the clearly typical sixfold symmetry that was considered for graphite/reduced oxied graphene. And the SAED of 10 without any points is shown in the inset of figure 1(f), supposed the PS chain was adhesed on the surfaces of rGO through the strong π–π interaction. From the TEM image of 10 which is shown in figure 1(f) it was observed kinds of different lamellas were stacked, confirming the PS chain was adhered on the surfaces of rGO again. The TEM–EDS patterns of 10 are shown in figure 1(g), corresponding peaks of C, O, and N atomic. The peak of N atomic demonstrated that N-doping was achieved by the DMF decomposition in the DMF solvothermal process. The results of the PS chain adhering on the surfaces of rGO and N-doping were also comfirmed by the XRD (figure 2), FTIR spectrometer (figure 4) and Raman microscopy (figure 5).

The XRD patterns of GO, and the 3D PS/rGO composite are shown in figure 2. The XRD pattern of the GO showed a notable peak at 10.22°, corresponding to an interplanar spacing of 8.66 Å, due to the chemical oxidation breaching the ordering of layers and bringing oxygen-containing groups such as epoxy, hydroxyl, carboxyl and carbonyl groups adhering on the GO sheets [28, 29]. The XRD pattern of PS shows two primary peaks. The first one around 10.30° is the polymerization peak which could be a result of the intermolecular backbone–backbone

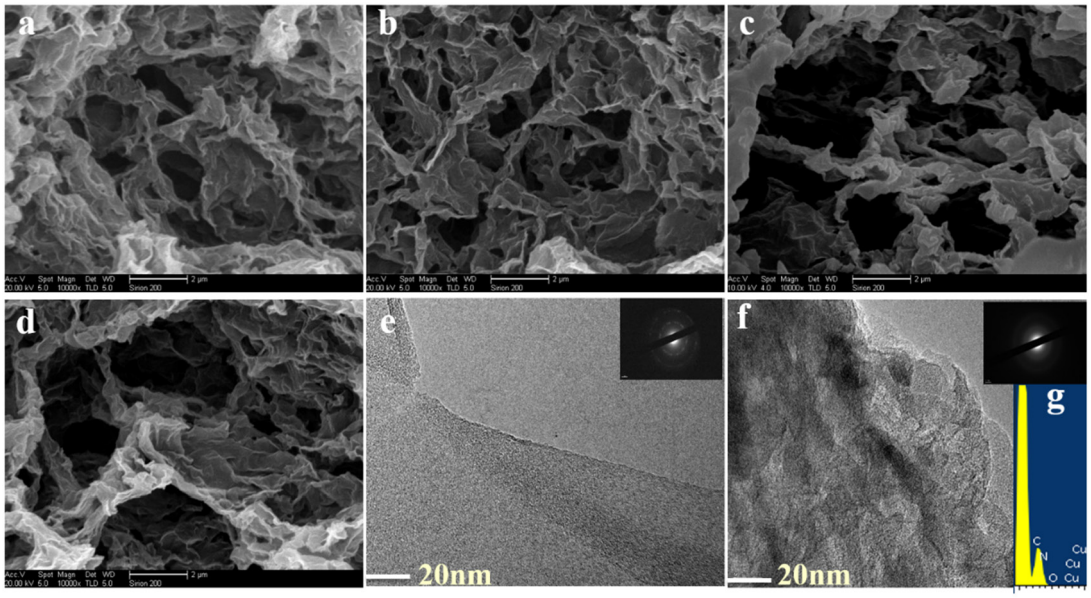

Figure 1. SEM images of (a) sample 4, (b) sample 6, (c) sample 8, (d) sample 10. TEM images of (e) GO, inserts show SAED, (f) 10, inserts show SAED. EDS patterns of (g) 10.

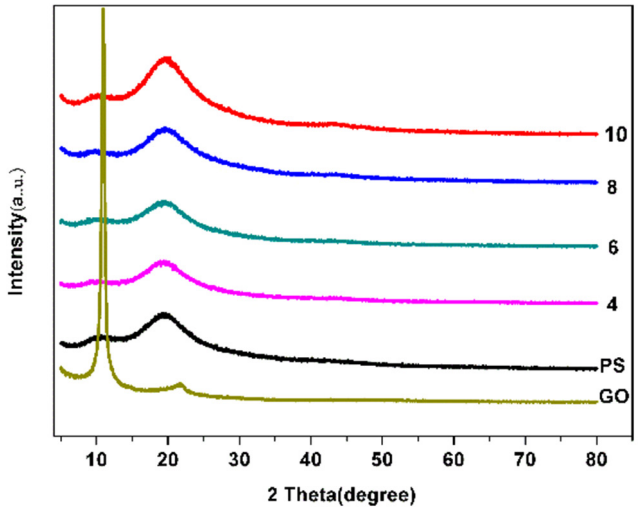

Figure 2. X-ray diffraction patterns of GO, PS, 4, 6, 8, 10.

mutuality and the size of the side groups, corresponding to a similar hexagonal ordering of the molecular chains. The other peak about 19° of the PS exhibits a broad diffraction peak, indicating that PS is basically amorphous in nature [30, 31]. In the XRD patterns of 10, 8, 6, 4 in figure 2, the diffraction peak of GO (10.22°) disappeared thoroughly after the DMF solvothermal reaction, indicating the solvothermal reaction is an effective method which could remove most of the oxygen-containing groups on the graphene oxide nanosheets [29]. Two peaks of these composites, which looked like the peaks of the PS, were observed in the figure 2. But the diffraction peaks of PS-rGO composites which have different concentration of GO have some changes compared to the pure PS, due to the PS chains binding and resulting from PS chains attached on the surfaces of rGO through the strong π–π interaction [32].

The XPS was employed to analyze the characteristics of the GO and the electronic states of N doped for PS/rGO composites. The survey XPS spectrums of the GO and the PS/rGO composites (sample 10) are shown in figure 3(a). The obvious O1s peak (533 eV) of the GO was observed, but sample 10 had a significantly weaker O1s peak than the GO (rectangular label in figure 3(a)) and presented a N1s peak (400.23 eV), indicating that the GO was an effective reduction and the N was doped into the composites during the DMF solvothermal process [33]. The C1s peak of the GO (figure 3(b)) was deconvoluted into five peaks, which were C–C (284.4 eV), C-OH (285.1 eV), C–O–C (286.5 eV), C=O (287.1 eV) and –O–C=O (287.9 eV), respectively [34, 35]. In figure 3(c), The C1s spectrum of the sample 10 could be split into two peaks, which were C–C (284.6 eV) and C–N (285.3 eV)

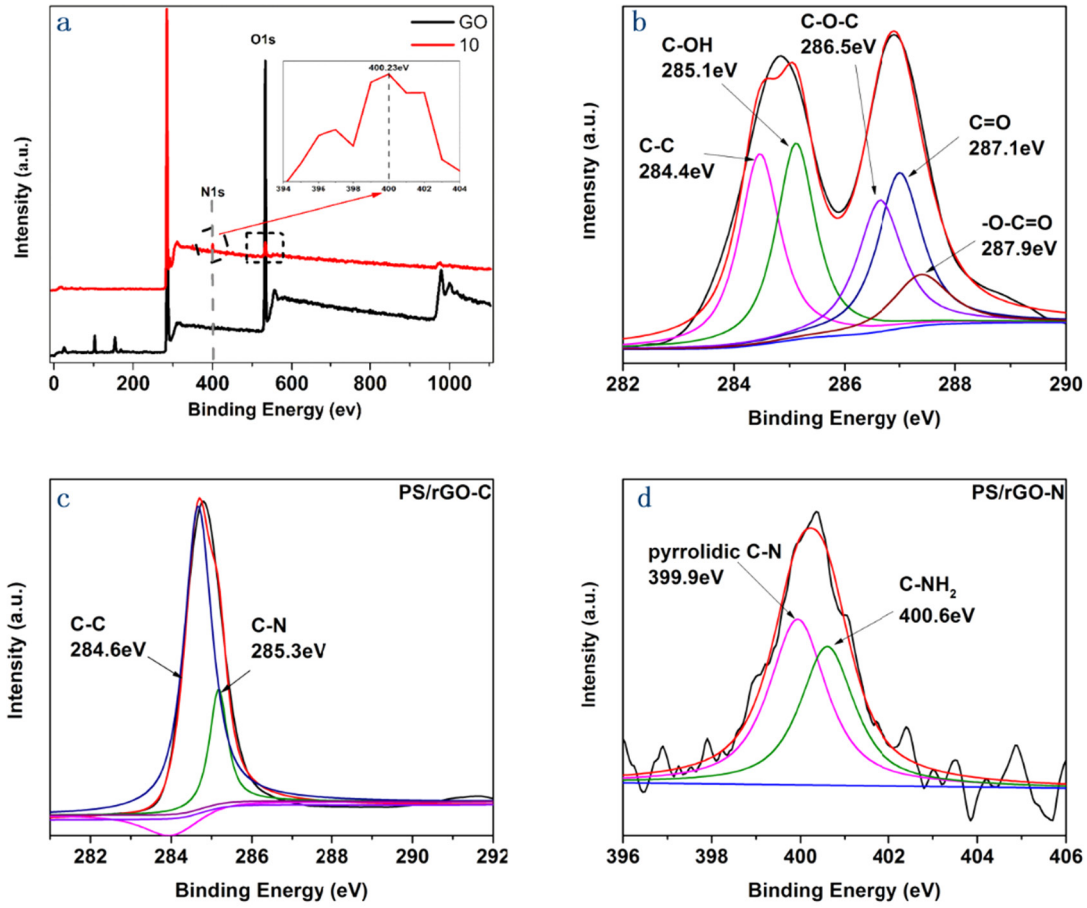

Figure 3. (a) Survey XPS spectrum of GO and composite 10; (b) C1s spectrum of the GO; XPS spectrum of composite 10 (c) C1s and (d) N1s.

respectively [36, 37]. Compared with the C1s of the Go and sample 10, the existence of the C–N could confirm the N doping. And the N1s deconvolution of sample 10 (figure 3(d)) showed the pyrrolidic C–N (399.9 eV) and C–NH_2 (400.6 eV) [38]. The result also confirmed the success for the N doping during the DMF solvothermal process. All the results could also indicate the DMF acting as the N-source, because the DMF was the only chemical containing nitrogen.

The FT-IR was used to indicate the existent of functional groups of the GO and PS/rGO composites. The spectroscopy are shown in figure 4. The pure PS shows the characteristic aromatic C = C stretching absorption peaks at 1600 cm^{-1}, 1492 cm^{-1} and 1452 cm^{-1}; the peaks around 696 cm^{-1} and 755 cm^{-1} are due to aromatic C = C bending and aromatic C–H bending, respectively [39]. The C–H stretching of the phenyl is around 3025 cm^{-1}, and the C–H stretching band of methylene and methenyl groups are about 2921, 2850 cm^{-1}, respectively [40, 41]. It could obviously be found that these composites (4, 6, 8, 10) also have similar absorption peaks as the pure PS. This result also proves that the PS twining and resulting from PS chains on the surfaces of rGO during the DMF solvothermal process. But it also found these composites have two new obvious absorption peaks at around 1178 cm^{-1} and 3400 cm^{-1} compared to the pure PS, due to C–N stretching vibration and N–H may be with the same O–H stretching vibrations, respectively. It might confirm the appearance of the C–NH–C bands, because the DMF was decomposed into carbon monoxide and dimethylamine during the DMF solvothermal process [20, 42]. Also, it successfully brought the N groups into the composites, realizing the N doping.

Figure 5 shows the Raman spectroscopy of GO and PS/rGO composites. The Raman spectroscopy could investigate the structure and quality of carbon materials, especially the defects and structures of graphene. In here, the Raman spectra of these samples were measured by Confocal Raman Microscopy at an excitation wavelength of 532 nm without any solvent. All of the samples show two representative Raman active peaks which were located at 1340–1348 cm^{-1} and 1589–1597 cm^{-1}, corresponding to the D and G modes respectively. The D band is known as the structural defects and disordered structures of the sp^2. And the G band is about the E_{2g}-vibration mode of sp^2 bonded carbon, which is the main active mode of the graphite and reflects the degree of graphitization [43]. The peaks of G of the 4, 6, 8, 10 (1597, 1590, 1591, 1590 cm^{-1}, respectively) were shown slight blue-shift to compare with the GO (1589 cm^{-1}), indicating the strong π–π interaction between PS and rGO [21]. Also, the integrated intensities ratio of the D and G band (I_D/I_G) of the 4, 6, 8, 10 (1.489, 1.451, 1.486, 1.453, respectively) were greater

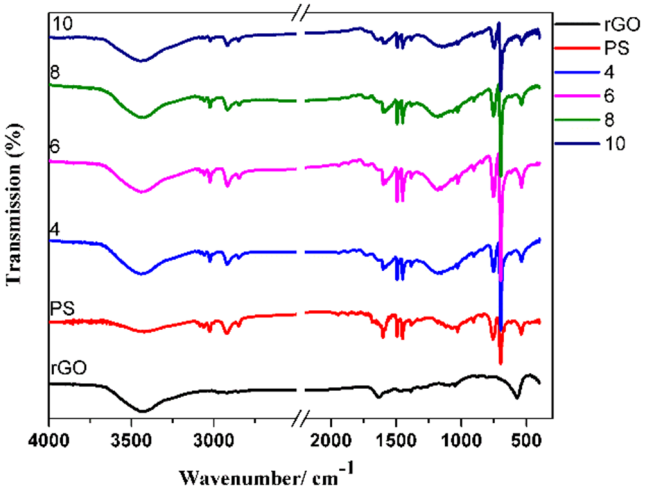

Figure 4. IR spectra of rGO, PS, 4, 6, 8, 10.

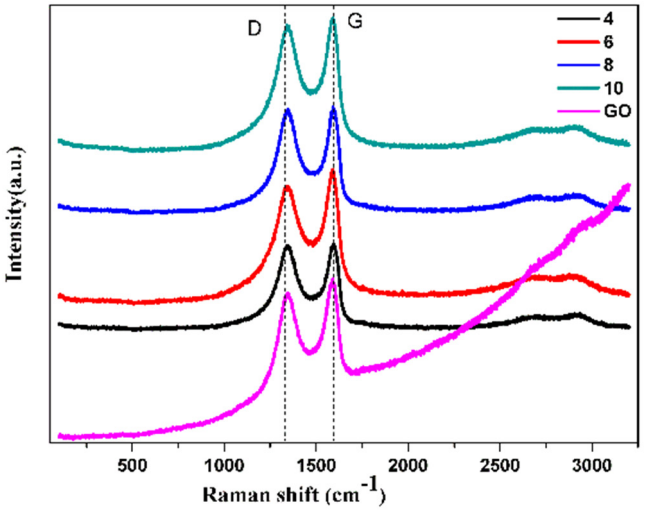

Figure 5. The Raman spectroscopy of 4, 6, 8, 10, GO.

than the GO (1.305), indicating that the GO was not only reduced, but produced more defects as a result of the strong π–π interaction between PS and rGO at the DMF solvothermal process.

3.3. Properties of PS/rGO composites

The curves of figure 6 were characterized in nitrogen condition by TGA, which was explained by the thermal stability of the 6, 8, 10, PS, rGO, and explored the influences of the rGO on the thermal stability of the composites. There could be split into three weight loss process. First, there was slight weight loss for the composites under 270 °C, due to few adsorbed solvent and the residual oxygen functional groups on the rGO sheets [26]. But the pure PS had no weight loss under 270 °C. Second, because the lower molecular of the all samples began to decompose from 270 to 370 °C, the weight loss was around 5%. In the last process, the samples were degraded over 374 °C, which might result from the decomposition of higher molecular of the PS [44]. Besides, the temperatures of the 80% weight loss ($T_{80\%}$) of the 6, 8, 10 were higher 11, 15, 16 °C than the pure PS, respectively. These results showed the thermal stability of the composites was higher than the pure PS, which may attribute to the strong π–π interaction between the PS and rGO sheets [45].

The room temperature conductivity of samples containing different amount of GO was illustrated in figure 7. The internal framework structure of PS/rGO composites with uniformly dispersed rGO network in the PS matrix causes their relatively high conductivity compared with the pure PS. The results show that the conductivity was increased by the amount of GO and the increment was obvious for the amount of GO less than 4 wt.%, indicating the percolation thresholds are in the intervals (lower than 4 wt.%) for the PS/rGO composites. In other words, this increment in the conductivity of these composites is controlled by the conducting rGO networks. The conductivity of 4 (1.57×10^{-2} S m^{-1}) was twelve orders of magnitude larger than the pure PS (1.5×10^{-14} S m^{-1})

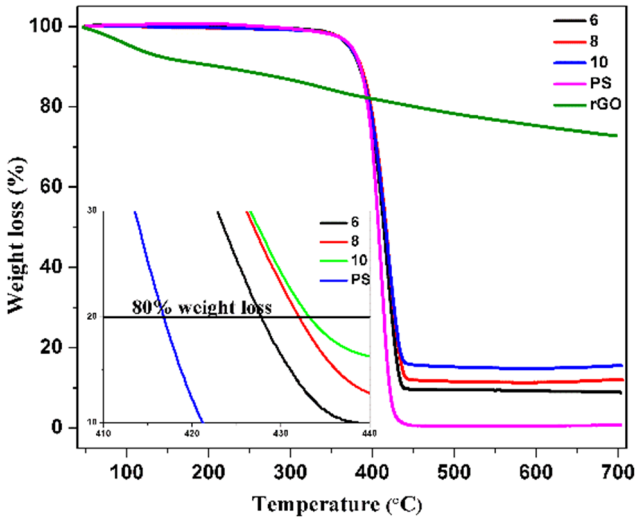

Figure 6. TGA curves of 6, 8, 10, PS, rGO.

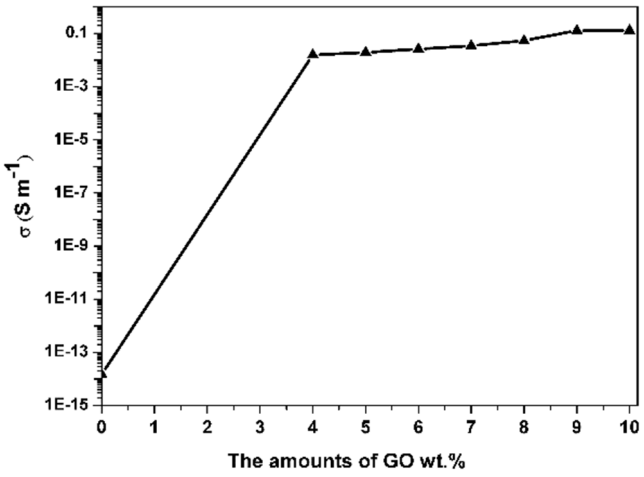

Figure 7. Electrical conductivity as a function of GO concentration for PS/rGO composites.

which is insulating and was higher than some reported references of graphene-based composites with some loading [46, 47]. The higher electrical conductivity of our 3D composites compare to the pure PS could be attributed to unique 3D pore structure and relatively high level N-doping. First, the 3D pore structure plays an important role in efficiently reducing the degree of restacking of graphene sheets, which could not only keep the high structural integrity of the sheets, but also provide continuous electron conduction pathways that were favorable for electron transport [48, 49]. Second, the abundance of doping N atoms may increase the concentration of the charge carriers, and further improve the ion transfer efficiency [50]. The relatively high conductivity of PS/rGO composites and the unique 3D structure could enhance the EMI shielding effectiveness of PS/rGO composites.

In general, the EMI shielding effectiveness (SE) of composites was related to factors such as frequency, thickness, dielectric properties and magnetic permeability [51]. It was noted the effect of frequency range from 1 to 9 GHz on the EMI SE of samples with different GO concentration in figure 8. The curves show EMI SE increased with a rise in the GO concentration. The result was similar to the electrical conductivity of the samples shown in figure 7. In other words, the shielding effectiveness of PS/rGO composites increased when electrical conductivity of composites were improved.

The total EMI SE (SE_T) was the sum of the absorption (SE_A), the reflection (SE_R) and the internal multiple reflection (SE_M) which was usually neglected when $SE_T \geqslant 10$ dB [52]. So it could be generally described as

$$SE_T \approx SE_A + SE_R + SE_M$$

For example, the SE_T, SE_A, and SE_R of the composite with 10 wt.% rGO were 15.57 dB, 14.48 dB and 1.09 dB at 9 GHz, respectively. It was indicated that the contribution of SE_A was a dominant role in the total EMI SE. Ling *et al* had presented that the EMI SE of microcellular polyetherimide/graphene composites foams were about 12 dB for

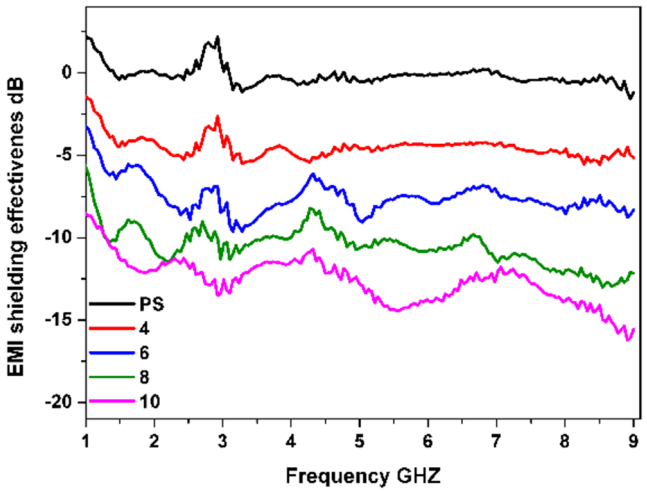

Figure 8. EMI shielding effectiveness as a function of GO concentration for PS/rGO composites.

10 wt.% graphene [53]. Li *et al* had reported the SE_T of polystyrene/functionalized graphene nanocomposite foams (10 wt.%, thickness of 2.88 mm) using supercritical carbon dioxide was about 15 dB at 9 GHz [46]. The EMI SE of 3D PS/rGO using a simple method in this work could be ascribed to the conductive fillers and 3D networks.

4. Conclusions

In this work, we focused on using a simple, versatile, facile, low-cost and environment-friendly one-step rational route for the preparation of 3D PS/rGO composites with N-doping, with no extra complicated chemical functional surfactants and N-doping agents. 3D structure brings a relatively high conductivity and thermal stability. The electrical and EMI measurement confirms the typical N-doped structure, which offers an effective way to tailor the properties of PS/rGO composites, thus making N-graphene a promising material for use in electronic devices.

Acknowledgments

The authors are grateful for the support of the Natural Science Foundation of China (Grant No. 51502293), Anhui Provincial Natural Science Foundation (1408085MB39, 1508085QE112, 1508085QE110) and Youth Innovation Promotion Association, CAS (2014288, 2015268).

Conflict of interest

The authors declare no conflict of interest.

References

[1] Chen W, Li S, Chen C and Yan L 2011 Self-assembly and embedding of nanoparticles by *in situ* reduced graphene for preparation of a 3D graphene/nanoparticle aerogel *Adv. Mater.* **23** 5679–83
[2] Singh K *et al* 2013 Nanostructured graphene/Fe3O4 incorporated polyaniline as a high performance shield against electromagnetic pollution *Nanoscale* **5** 2411–20
[3] Cao M-S, Wang X-X, Cao W-Q and Yuan J 2015 Ultrathin graphene: electrical properties and highly efficient electromagnetic interference shielding *J. Mater. Chem.* C **3** 6589–99
[4] Wu Q, Xu Y X, Yao Z Y, Liu A R and Shi G Q 2010 Supercapacitors based on flexible graphene/polyaniline nanofiber composite films *ACS Nano* **4** 1963–70
[5] Bi H C, Xie X, Yin K B, Zhou Y L, Wan S, He L B, Xu F, Banhart F, Sun L T and Ruoff R S 2012 Spongy graphene as a highly efficient and recyclable sorbent for oils and organic solvents *Adv. Funct. Mater.* **22** 4421–25
[6] Luo J, Zhong W, Zou Y, Xiong C and Yang W 2016 Preparation of morphology-controllable polyaniline and polyaniline/graphene hydrogels for high performance binder-free supercapacitor electrodes *J. Power Sources* **319** 73–81
[7] Yu M, Huang Y, Li C, Zeng Y, Wang W, Li Y, Fang P, Lu X and Tong Y 2015 Building three-dimensional graphene frameworks for energy storage and catalysis *Adv. Funct. Mater* **25** 324–30
[8] Li C and Shi G 2012 Three-dimensional graphene architectures *Nanoscale* **4** 5549–63
[9] Xu Y, Shi G and Duan X 2015 Self-assembled three-dimensional graphene macrostructures: synthesis and applications in supercapacitors *Acc. Chem. Res.* **48** 1666–75
[10] Chen Z, Ren W, Gao L, Liu B, Pei S and Cheng H M 2011 Three-dimensional flexible and conductive interconnected graphene networks grown by chemical vapour deposition *Nat. Mater.* **10** 424–8

[11] Xia X H, Chao D L, Zhang Y Q, Shen Z X and Fan H J 2014 Three-dimensional graphene and their integrated electrodes *Nano Today* **9** 785–807
[12] Sun M, Li H, Wang J and Wang G 2015 Promising graphene/carbon nanotube foam@π-conjugated polymer self-supporting composite cathodes for high-performance rechargeable lithium batteries *Carbon* **94** 864–71
[13] Zhang H, Xie A, Wang C, Wang H, Shen Y and Tian X 2013 Novel rGO/α-Fe2O3 composite hydrogel: synthesis, characterization and high performance of electromagnetic wave absorption *J. Mater. Chem.* A **1** 8547
[14] Wu F, Xia Y, Wang Y and Wang M 2014 Two-step reduction of self-assembed three-dimensional (3D) reduced graphene oxide (RGO)/zinc oxide (ZnO) nanocomposites for electromagnetic absorption *J. Mater. Chem.* A **2** 20307–15
[15] Worsley M A *et al* 2012 Mechanically robust 3D graphene macroassembly with high surface area *Chem. Commun.* **48** 8428–30
[16] Niu Z, Chen J, Hng H H, Ma J and Chen X 2012 A leavening strategy to prepare reduced graphene oxide foams *Adv. Mater.* **24** 4144–50
[17] Sathish M, Mitani S, Tomai T and Honma I 2014 Supercritical fluid assisted synthesis of N-doped graphene nanosheets and their capacitance behavior in ionic liquid and aqueous electrolytes *J. Mater. Chem.* A **2** 4731
[18] Wei D C, Liu Y Q, Wang Y, Zhang H L, Huang L P and Yu G 2009 Synthesis of N-doped graphene by chemical vapor deposition and its electrical properties *Nano Lett.* **9** 1752–58
[19] Marcano D C, Kosynkin D V, Berlin J M, Sinitskii A, Sun Z Z, Slesarev A, Alemany L B, Lu W and Tour J M 2010 Improved synthesis of graphene oxide *ACS Nano* **4** 4806–14
[20] Su Z, Wang H, Tian K, Xu F, Huang W and Tian X 2016 Simultaneous reduction and surface functionalization of graphene oxide with wrinkled structure by diethylenetriamine (DETA) and their reinforcing effects in the flexible poly(2-ethylhexyl acrylate) (P2EHA) films *Composites* A **84** 64–75
[21] Chen L, Wang X, Zhang X and Zhang H 2012 3D porous and redox-active prussian blue-in-graphene aerogels for highly efficient electrochemical detection of H_2O_2 *J. Mater. Chem.* **22** 22090–96
[22] Zhang Y, Sun H, Zhang W, Gao Z, Yang P and Gu J 2015 N,N-dimethylformamide solvothermal strategy: from fabrication of palladium nanoparticles supported on reduced graphene oxide nanosheets to their application in catalytic aminocarbonylation reactions *Appl. Catal.* A **496** 9–16
[23] Ai K, Liu Y, Lu L, Cheng X and Huo L 2011 A novel strategy for making soluble reduced graphene oxide sheets cheaply by adopting an endogenous reducing agent *J. Mater. Chem.* **21** 3365–70
[24] Xu Y, Sheng K, Li C and Shi G 2010 Self-assembled graphene hydrogel via a one-step hydrothermal process *ACS Nano* **4** 4324–30
[25] Ye S and Feng J 2014 Self-assembled three-dimensional hierarchical graphene/polypyrrole nanotube hybrid aerogel and its application for supercapacitors *ACS Appl. Mater. Interfaces* **6** 9671–9
[26] Guo D, Cai P, Sun J, He W, Wu X, Zhang T, Wang X and Zhang X 2016 Reduced-graphene-oxide/metal-oxide p-n heterojunction aerogels as efficient 3D sensing frameworks for phenol detection *Carbon* **99** 571–78
[27] Yang H, Wang N, Xu Q, Chen Z, Ren Y, Razal J M and Chen J 2014 Fabrication of graphene foam supported carbon nanotube/polyaniline hybrids for high-performance supercapacitor applications *2d Mater.* **1** 034002
[28] Zhang L, Chen G, Hedhili M N, Zhang H and Wang P 2012 Three-dimensional assemblies of graphene prepared by a novel chemical reduction-induced self-assembly method *Nanoscale* **4** 7038
[29] Zhang F, Xiao F, Dong Z H and Shi W 2013 Synthesis of polypyrrole wrapped graphene hydrogels composites as supercapacitor electrodes *Electrochim. Acta* **114** 125–32
[30] Liu Z, Yan J, Miao Y-E, Huang Y and Liu T 2015 Catalytic and antibacterial activities of green-synthesized silver nanoparticles on electrospun polystyrene nanofiber membranes using tea polyphenols *Composites* B **79** 217–23
[31] She X, Liu T, Wu N, Xu X, Li J, Yang D and Frost R 2013 Spectrum analysis of the reduction degree of two-step reduced graphene oxide (GO) and the polymer/r-GO composites *Mater. Chem. Phys.* **143** 240–46
[32] Kumar A, Bansal A, Behera B, Jain S L and Ray S S 2016 Ternary hybrid polymeric nanocomposites through grafting of polystyrene on graphene oxide-TiO_2 by surface initiated atom transfer radical polymerization (SI-ATRP) *Mater. Chem. Phys.* **172** 189–96
[33] Liu Q, Guo B, Rao Z, Zhang B and Gong J R 2013 Strong two-photon-induced fluorescence from photostable, biocompatible nitrogen-doped graphene quantum dots for cellular and deep-tissue imaging *Nano Lett.* **13** 2436–41
[34] Wang H, Maiyalagan T and Wang X 2012 Review on recent progress in nitrogen-doped graphene: synthesis, characterization, and its potential applications *ACS Catal.* **2** 781–94
[35] Qu D, Zheng M, Li J, Xie Z and Sun Z 2015 Tailoring color emissions from N-doped graphene quantum dots for bioimaging applications *Light Sci. Appl.* **4** e364
[36] Bao J F, Kishi N and Soga T 2014 Synthesis of nitrogen-doped graphene by the thermal chemical vapor deposition method from a single liquid precursor *Mater. Lett.* **117** 199–203
[37] Kao W Y, Chen W Q, Chiu Y H, Ho Y H and Chen C H 2016 General solvent-dependent strategy toward enhanced oxygen reduction reaction in graphene/metal oxide nanohybrids: effects of nitrogen-containing solvent *Sci. Rep.* **6** 37174
[38] Seo S, Yoon Y, Lee J, Park Y and Lee H 2013 Nitrogen-doped partially reduced graphene oxide rewritable nonvolatile memory *ACS Nano* **7** 3607–15
[39] Yu Y-H, Lin Y-Y, Lin C-H, Chan C-C and Huang Y-C 2014 High-performance polystyrene/graphene-based nanocomposites with excellent anti-corrosion properties *Polym. Chem.* **5** 535–50
[40] Liaw W-C, Cheng Y-L, Chang M-K, Lien W-F and Lai H-R 2015 The preparation of Ni-plated polystyrene microspheres using 3-(trimethoxysilyl) propyl methacrylate as a bridging agent *Polym. J.* **48** 91–9
[41] Fan X, Zheng L, Cheng J, Xu S, Wen X, Cai Z, Pi P and Yang Z 2012 Template synthesis of raspberry-like polystyrene/SiO_2 composite microspheres and their application in wettability gradient surfaces *Surf. Coat. Technol.* **213** 90–7
[42] Ma H-L, Zhang H-B, Hu Q-H, Li W-J, Jiang Z-G, Yu Z-Z and Dasari A 2012 Functionalization and reduction of graphene oxide withp-phenylene diamine for electrically conductive and thermally stable polystyrene composites *ACS Appl. Mater. Interfaces* **4** 1948–53
[43] Some S, Bhunia P, Hwang E, Lee K, Yoon Y, Seo S and Lee H 2012 Can commonly used hydrazine produce n-type graphene? *Chemistry* **18** 7665–70
[44] Patole A S, Patole S P, Kang H, Yoo J B, Kim T H and Ahn J H 2010 A facile approach to the fabrication of graphene/polystyrene nanocomposite by *in situ* microemulsion polymerization *J. Colloid Interface Sci.* **350** 530–7
[45] Kassaee M Z, Motamedi E and Majdi M 2011 Magnetic Fe_3O_4-graphene oxide/polystyrene: Fabrication and characterization of a promising nanocomposite *Chem. Eng. J.* **172** 540–49
[46] Li C Q, Yang G H, Deng H, Wang K, Zhang Q, Chen F and Fu Q 2013 The preparation and properties of polystyrene/functionalized graphene nanocomposite foams using supercritical carbon dioxide *Polym. Int.* **62** 1077–84

[47] Liang J, Wang Y, Huang Y, Ma Y, Liu Z, Cai J, Zhang C, Gao H and Chen Y 2009 Electromagnetic interference shielding of graphene/epoxy composites *Carbon* **47** 922–5
[48] Liu Y, Wang X, Wan W, Li L, Dong Y, Zhao Z and Qiu J 2016 Multifunctional nitrogen-doped graphene nanoribbon aerogels for superior lithium storage and cell culture *Nanoscale* **8** 2159–67
[49] Odedairo T, Ma J, Gu Y, Zhou W, Jin J, Zhao X S and Zhu Z 2014 A new approach to nanoporous graphene sheets via rapid microwave-induced plasma for energy applications *Nanotechnology* **25** 10
[50] Ma X, Ning G, Sun Y, Pu Y and Gao J 2014 High capacity Li storage in sulfur and nitrogen dual-doped graphene networks *Carbon* **79** 310–20
[51] Singh A P, Mishra M, Sambyal P, Gupta B K, Singh B P, Chandra A and Dhawan S K 2014 Encapsulation of gamma-Fe_2O_3 decorated reduced graphene oxide in polyaniline core-shell tubes as an exceptional tracker for electromagnetic environmental pollution *J. Mater. Chem.* A **2** 3581–93
[52] Suilin S, Lingzhen Z and Junshou L 2009 Complex permittivity and electromagnetic interference shielding properties of Ti_3SiC_2/polyaniline composites *J. Mater. Sci.* **44** 945–48
[53] Ling J, Zhai W, Feng W, Shen B, Zhang J and Zheng W 2013 Facile preparation of lightweight microcellular polyetherimide/graphene composite foams for electromagnetic interference shielding *ACS Appl. Mater. Interfaces* **5** 2677–84